International Journal of Microwave and Wireless Technologies, 2017, 9(1), 151–162.
doi:10.1017/S1759078715000975

RESEARCH PAPER

A CPW-fed stepped slot UWB antenna for MIMO/diversity applications

RAJ KUMAR[1] AND NEHA PAZARE[2]

An ultra-wideband (UWB) slot antenna for diversity applications is introduced. The overall structure of the antenna consists of two similar coplanar waveguide (CPW)-fed stepped rectangular slots placed in an orthogonal position. The slots are asymmetric with respect to their placement in the ground plane. The CPW feeds are double stepped and terminated on hexagonal patches for better impedance matching. A wide impedance bandwidth (measured) from 3 to 12 GHz with an isolation better than 15 dB is obtained with this antenna. To improve the isolation, the design is modified and an I-shaped slot strip is introduced between the two slot antennas. With this, the isolation is brought about 25 dB of most of the band, while the impedance bandwidth remains the same (2.8–12 GHz for port 1, measured and 2.9–12 GHz for port 2, measured). The far-field radiation patterns are also measured and a peak gain of about 5 dBi is obtained. Finally, the diversity parameters such as envelope correlation coefficient and capacity loss are calculated and found to have low values. The antenna is expected to be useful for UWB diversity applications with good isolation.

Keywords: Slot antenna, Multi-input multi-output, Polarization diversity, UWB antenna

Received 24 January 2015; Revised 25 April 2015; Accepted 30 April 2015; first published online 1 June 2015

I. INTRODUCTION

Wireless communication in a scattering environment consisting of trees, buildings, walls, and other obstacles suffers from fading due to multipath and the consequent loss of information [1, 2]. Antenna diversity in which two or more antennas are used is a useful technique, which can overcome this problem. Antenna diversity can be implemented in mobile wireless communication systems as well as at base stations [3–6]. In case of mobile or compact wireless equipment, due to physical space constraints, antennas are closely placed which gives rise to problems of mutual coupling and correlation between signals. To lower the mutual coupling, some of the methods used are; inserting metallic reflectors between the two antennas, optimizing the separation or arrangement of the antennas, and orienting the antennas such that their electric fields are at right angles to each other.

Some of the diversity antennas proposed recently are reported in [7–13]. In [7], two 52×54 mm^2 sized fork-shaped quad band coplanar waveguide (CPW)-fed monopole antennas were orthogonally placed with an inverted U-shaped strip for polarization diversity. It has $S_{11} < -10$ dB centered at 1.9, 2.4, 3.5, and 5.5 GHz and coupling < -22 dB over the operation region. A dual-band microstrip fed slot antenna for wireless local area network (WLAN)/ultra-wideband (UWB) is presented as diversity antenna in [8]. The described antenna has a U-shaped patch, a T-shaped monopole, and a pentagonal wide slot in the ground plane. The antennas were tested in four different spatial arrangements and the results were compared. The overall size of the antenna was 28×56 mm^2. The antenna can work for WLAN (2.4–2.485 GHz) and UWB (3.1–10.6 GHz) ranges having S_{11} below -10 dB. The coupling for the best arrangement is < -20 dB. An array of E-shaped printed monopole multiband antennas of individual size 35×38 mm^2 for multiple-input–multiple-output (MIMO)/diversity system is proposed in [9]. The antenna covers WLAN band of 2.4, 5.4, and 5.8 GHz with isolation more than 14 dB. In [10], the mutual coupling between two circular monopole antennas operating over the frequency range of 3.2–10.6 GHz is lowered using an inverted Y-shaped stub, which is placed at the middle of the ground plane. Mutual coupling of < -15 dB is achieved with antenna size of 68×40 mm^2. An UWB MIMO antenna with a size of 35×40 mm^2 in [11] has used a tree-like structure to reduce the coupling to below -16 dB over the operating band of 3.1–10.6 GHz. In [12], a T-shaped protruded ground plane is placed in between two radiators to obtain a coupling of $S_{21} < -20$ dB for the operating range of 2.3–7.7 GHz. The size of antenna is 48×115 mm^2. In [13], three stubs are placed between the antenna ports with the size of antenna being 80×60 mm^2 and an isolation of 20 dB is achieved for an impedance bandwidth of 2.27–10.2 GHz. A comparison of the performance of the antennas mentioned in the references with the proposed antenna is made in Table 1. From the table it can be seen that the proposed antenna is compact, has wider bandwidth and better isolation than the antennas described in the references.

[1]ARDE, Pashan, Pune 411 021, India
[2]DIAT (DU), Girinagar, Pune 411 025, India
Corresponding author:
R. Kumar
Email: raj34_shivani@yahoo.co.in

Table 1. Comparison of performance of proposed antenna with references.

Sl no.	References	Antenna size (mm²)	Bandwidth (GHz)	Isolation (dB)
1	[7]	108 × 54	Narrow bands centered at 1.9, 2.4, 3.5, and 5.5	22
2	[8]	28 × 56	2.4–2.485 and 3.1–10.6	20
3	[9]	38 × 70	Narrow bands centered at 2.4, 5.4, and 5.8	14
4	[10]	68 × 40	3.2–10.6	15
5	[11]	35 × 40	3.1–10.6	16
6	[12]	48 × 115	2.3–7.7	20
7	[13]	80 × 60	2.27–10.2	20
8	Proposed	30 × 60	2.9–12	25

The proposed antenna for diversity applications consists of a stepped CPW-fed asymmetric rectangular slot excited with a hexagonal patch and two such antennas are placed orthogonally to each other to form the array. To improve the isolation, an I-shaped strip is placed between the two antennas. The proposed antenna can be operated over a wide range of 2.9–12 GHz covering beyond the Federal Communications Commission (FCC) band of 3.1–10.6 GHz. The isolation S_{21} better than 25 dB is achieved over much of the operating bandwidth. The proposed antenna will be useful for WLAN, wireless personal area networks, and wireless body area networks applications operating in the UWB region and where dense multipath environment exists. In Section II, antenna geometry is described followed by simulated and measured results in Section III, parametric studies in Section IV, radiation patterns and gain in Section V, and diversity parameters in Section VI. Finally, conclusions are made.

II. ANTENNA GEOMETRY

Two antennas are designed; antennas 1 and 2 whose geometries are shown in Fig. 1. Both the antennas are printed on FR4 substrate, which has relative permittivity of $\varepsilon_r = 4.4$, loss tangent of 0.025, and thickness of 1.6 mm. The overall size of antennas 1 and 2 is 30 × 60 mm². The basic structure in each of the antennas consists of two slots placed orthogonally. The physical details of the individual slot of antenna 2 (proposed antenna) is shown in Fig. 1(c). The slot in antenna 1 has almost similar structure but with slightly different dimensions and the addition or absence of an extra cut on the boundary. As can be seen from the figure, the slot is excited by a hexagonal patch of sides A mm and B mm and fed by a stepped CPW. The stepped CPW has lower feed width of 2.4 mm and upper feed width of 1.8 mm. Further, the hexagon is not regular but the opposite sides are of equal length. The gap between the

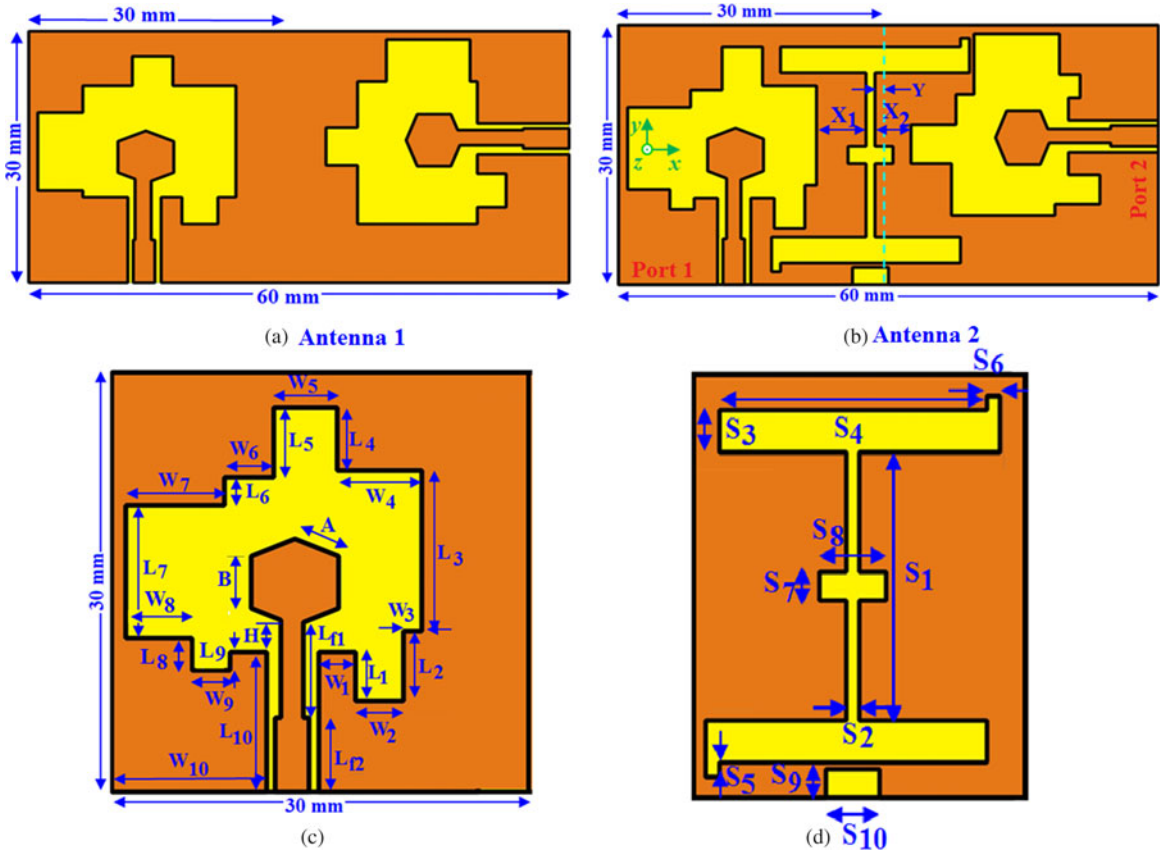

Fig. 1. (a) Geometry of antenna 1, (b) geometry of antenna 2, (c) slot details, and (d) isolation stub.

https://doi.org/10.1017/S1759078715000975 Published online by Cambridge University Press

feed and the ground plane is 0.6 mm at the lower end and 0.8 mm at the upper/patch end from the left side of ground plane. The stepped feed of asymmetric type is used to match the 50 Ω impedance of the connector with the high impedance of the patch. The placement of the slot in the ground plane is asymmetric, i.e. the ground clearance is more on the right side of the slot, whereas it is less on the left side of it. This is done to reduce the slot impedance and improve the matching.

In antenna 2, the mutual coupling between both the antenna ports is reduced by means of an isolation stub. The I-shaped stub whose details are given in Fig. 1(d) is placed exactly between the two nearest edges of the antenna because of which an offset of Y is introduced between the isolation stub and the center of the substrate. The position of the isolation stub from the antenna edges is given by X_1 and X_2. To further increase the isolation, a rectangular stub of $S_8 \times S_7$ is placed in the middle (vertically) of the isolation stub. In addition to it, a rectangular slot of size $S_9 \times S_{10}$ is placed below the isolation stub. However, with the addition of the isolation stub, the impedance matching is found to slightly get disturbed. Hence, some parameters are modified to get the desired results. The feed width on the connector side is modified to 2.4 mm and on the patch side is modified to 1.6 mm. Further, the feed is made symmetric and the gap between the ground plane and the feed is 1.6 mm on the patch side and 1.0 mm on the connector side. An additional slot is also made on the left side of the lower end of the ground plane to further improve the impedance bandwidth of antenna 2 as compared with antenna 1. The orientation of both the antennas in the co-ordinate axis system is shown in Fig. 1(b). The optimized dimensions of both the antennas are represented in tabular form in Table 2.

III. SIMULATED AND MEASURED RESULTS

Antennas 1 and 2 were optimized on electromagnetic solver and then fabricated. The return loss and isolation for the fabricated antennas was measured on a vector network analyzer (Rohde and Schwarz ZVA-40). The simulated and measured return losses and isolation for antennas 1 and 2 are compared and shown in Figs 2(a) and 2(b), respectively. In these figures, the isolation is the negative of the S_{21} parameter. The comparision shows that the measured results are having proper agreement with the simulated results. The differences between the two curves (simulated and measured) and some frequency shifts are due to the reflections from the Sub-Miniature version A (SMA) connector and the substrate having some uncertainty in its electrical properties. The measured impedance bandwidth is noted from 3 to 12 GHz at both the ports for antenna 1. The impedance bandwidth for antenna 2 is from 2.8 to 12 GHz at port 1 and 2.9 to 12 GHz for port 2. In case of antenna 1, the isolation is around 16 dB at lower frequency and becomes better than 20 dB after 5 GHz. The addition of the I-shaped slot in antenna 2 reduced the mutual coupling between the radiators to below −20 dB at lower frequencies and below −25 dB after 5.5 GHz. A comparision of the simulated and measured isolations of antennas 1 and 2 is also seperately shown in Fig. 2(c). From the figure, it can be seen that an overall improvement in the isolation is achieved with the addition of the I-shaped slot. The simulated S_{11} of a single-slot antenna having the same dimensions as that used in antenna 1 is compared with the simulated S_{11} and S_{22} of antenna 1 in Fig. 2(d).

IV. RESONANCE FREQUENCY CALCULATION

In case of both the antennas, several ressonances can be seen from the simulated S_{11} and S_{22} curves. Generally, the first two resonances can be obtained from the perimeter of the slot and the height of the patch. For antenna 2, port 2, these resonances are seen to be at 3.2 and 5 GHz. Following calculations give the description of resonances which are dependent on the antenna parameters. The first resonance frequency (f_1) is due to the effective perimeter of the slot made in the ground plane $S_{per,eff}$ and can be calculated using equation (1):

$$f_1 = \frac{c}{S_{per}\sqrt{\varepsilon_{r,eff}}}, \tag{1}$$

$$S_{per,eff} = L_3 + L_6 + L_7 + W_1 + W_3 + W_4 + W_7 + W_8 + W_1 = 50.7 \text{ mm},$$

$$\varepsilon_{r,eff} = \frac{\varepsilon_r + 1}{2},$$

where $\varepsilon_r = 4.4$ and c = velocity of light in free space = 3×10^8 m/s.

This second resonating frequency (f_2) depends upon the height of the patch and can be calculated as shown below

Table 2. Optimized dimension of antenna (mm).

Label	Antenna 1	Antenna 2	Label	Antenna 1	Antenna 2	Label	Antenna 2
L_1	3.2	3.5	W_1	2.3	2.6	S_1	19
L_2	3.2	5	W_2	4	3.4	S_2	1
L_3	13.3	11.5	W_3	2	1.3	S_3	3
L_4	3.5	4.5	W_4	7	6	S_4	20
L_5	3.5	5	W_5	4.5	4.5	S_5	1
L_6	3.2	2	W_6	5.5	3.5	S_6	1
L_7	9.3	9.5	W_7	5	7	S_7	2
L_8	0.8	2.3	W_8	5	4.7	S_8	5
L_9	–	1.3	W_9	5	2.7	S_9	2
L_{10}	10.2	10	W_{10}	11	11	S_{10}	4
L_{f1}	7.4	6.8	L_{f2}	5.1	5.3	X_1	5.5
A	3.33	3.33	H	2.1	2.3	X_2	4
B	3.74	3.74	–	–	–	Y	1.5

https://doi.org/10.1017/S1759078715000975 Published online by Cambridge University Press

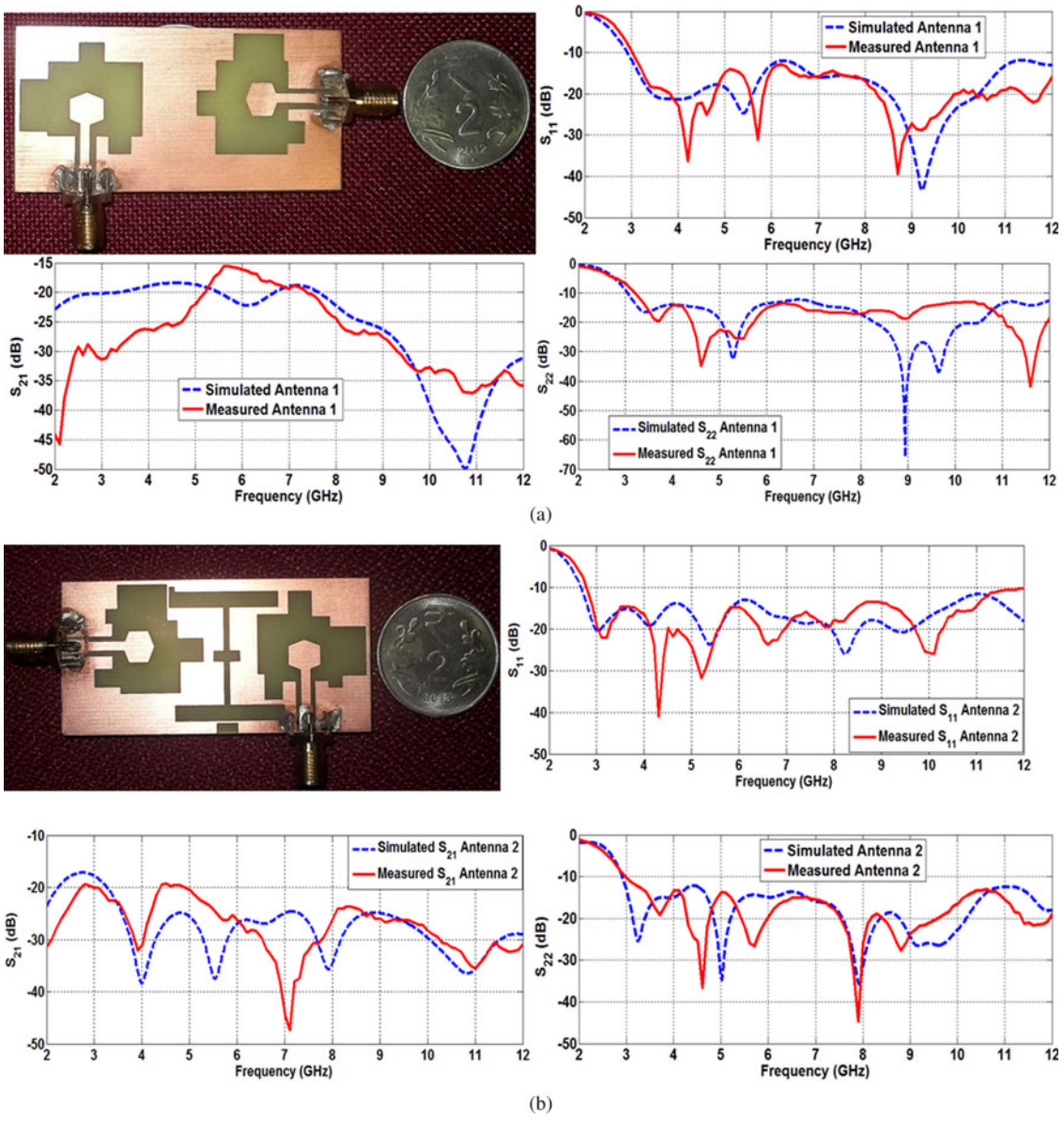

Fig. 2. (a) Photograph of antenna and measured and simulated *S*-parameters for antenna 1. (b) Photograph of antenna and measured and simulated *S*-parameters for antenna 2 (proposed). (c) Comparision of simulated and measured S_{21} of antennas 1 and 2. (d) Comparison of simulated return loss of antenna 1 (single slot, ports 1 and 2).

using equation (2):

$$f_2 = \frac{c}{4h\sqrt{\varepsilon_{r,eff}}}, \tag{2}$$

where h = effective height of the patch and $h \approx H + 2A = 8.9$ mm.

Hence the calculated values of first and second resonating frequencies come out to be 3.6 and 5.5 GHz, respectively, which nearly match with the simulated values of antenna 2 (with port 2), first and second resonating frequencies 3.2 and 5.13 GHz, respectively. The calculated and simulated values of the first resonance frequency show some difference due to the approximation in the slot length during calculation. The higher resonances (such as at 9.8 and 13.2 GHz) are harmonics of the first and second resonating frequencies which together merge to form the UWB characteristic of the antenna.

V. IMPROVEMENT IN ISOLATION

The improvement in the isolation with the various design stages (I–VI) is depicted in Fig. 3. In the figure, the solid blue curve gives the simulated isolation of antenna I, which is nearly 20 dB over most of the band. With the addition of a narrow rectangular slit 19 mm long and 1 mm wide (design stage II), the isolation is slightly improved near 5 GHz, i.e. approximately at the frequency where the slot is of $\lambda_{eff}/2$ length. When the narrow rectangular slit is modified into an I-shape structure (design stage III, dotted pink line), the isolation is brought above 25 dB over several frequencies. A little modification in the I-shape structure (addition of small

https://doi.org/10.1017/S1759078715000975 Published online by Cambridge University Press

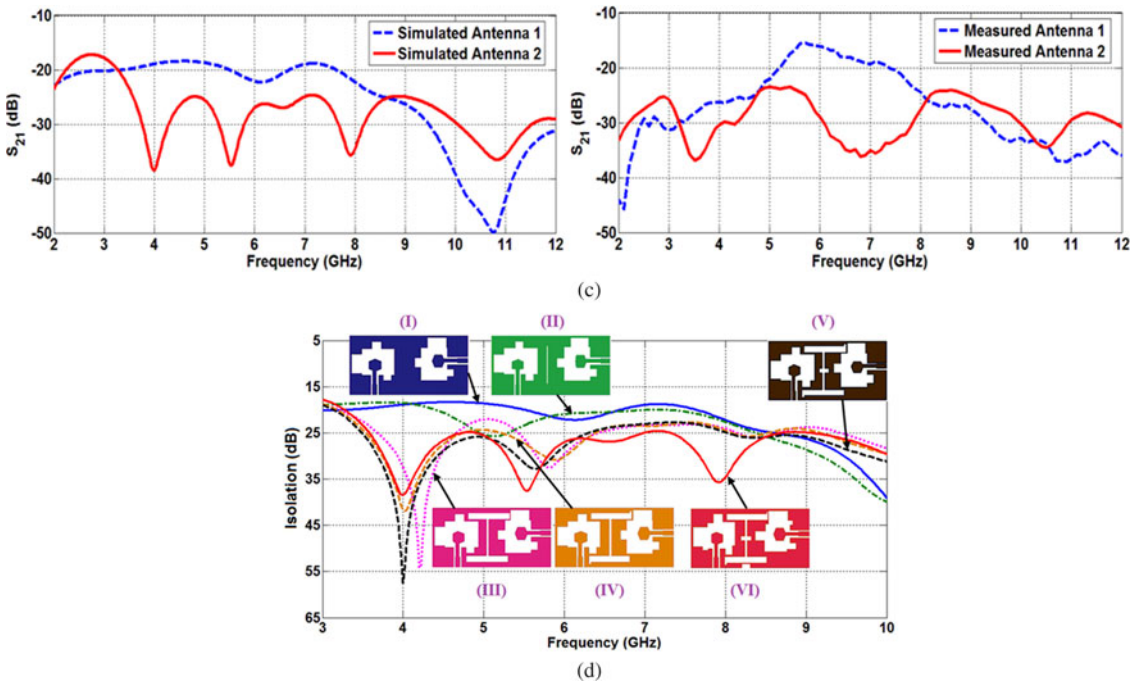

Fig. 2. (continued)

stubs at the upper and lower corners and horizontal stub in the middle) is done in stages IV and V, whereby there is further improvement in isolation at some frequencies (such as at 4 GHz). Finally in the last stage (stage VI), a small slot stub is added at the bottom edge of the ground plane and the overall slot structure of the antenna is slightly modified. This brings the simulated isolation to more than 25 dB throughout the band along with good return loss characteristics (Fig. 2(c), S_{11}, and S_{22} of antenna 2).

A plot of the surface current distribution for the two antennas (antennas 1 and 2) at some of the frequencies is shown in Fig. 4. These current distributions are obtained with port 1 (vertical feed on the left side) excitation and show the effect of the introduced I-shape structure in case of antenna 2 (figures in the bottom row). It is seen that at 4.2 GHz, in case of the antenna without the I-shaped stub, some current is found on the feed connected with port 2. With the addition of the I-shaped stub, a large current appears around the upper horizontal stub of the I-shaped structure. This reduces the coupling to port 2 as seen from the reduced current on the feed connected to port 2. The same is also noted from Fig. 3 where the isolation at 4.2 GHz was about 17 dB without the stub and reaches near 35 dB with the addition of the stub. Similarly, at 5 and 6.5 GHz, the induction of currents around the top and bottom horizontal sections of the I-shape stub reduces the currents on the other side feed. Finally, at 8.2 GHz, it is the bottom horizontal stub of the I-shape structure which absorbs much of the current and reduces the coupling.

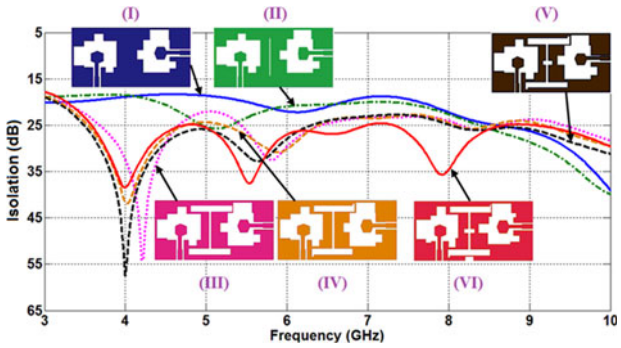

Fig. 3. Improvement in isolation with different design stages.

VI. PARAMETRIC RESULTS AND DISCUSSION

A parametric study is done to analyze the results with different parameter values and obtain the optimum values to get the desired performance. The effects of the different design parameters on the *S*-parameters are given below.

A) Depth of lower right slot stub

The design was simulated for different values of L_2 to examine its effect on the return loss and isolation (−ve of S_{21}). As shown in Fig. 5(a), by decreasing the depth of the stub, S_{11} was found to be degrading at lower frequencies (3–4 GHz). More importantly, isolation was also degrading near 6 GHz for lower values of L_2 as shown in Fig. 5(b). Hence L_2 was fixed at 5 mm. Increase of L_2 was not possible further because of geometry constraints.

B) Width of lower right slot stub

In Fig. 6, the variations in *S*-parameters for different values of W_2 are shown. In Fig. 7(a), it can be seen that when W_2 is decreased, the return loss deteriorates at some frequencies and a notch at approximately 10 GHz becomes more prominent with the return loss increasing to nearly 5 dB. W_2 was fixed at 3.4 mm and further increasing its width deteriorates the

https://doi.org/10.1017/S1759078715000975 Published online by Cambridge University Press

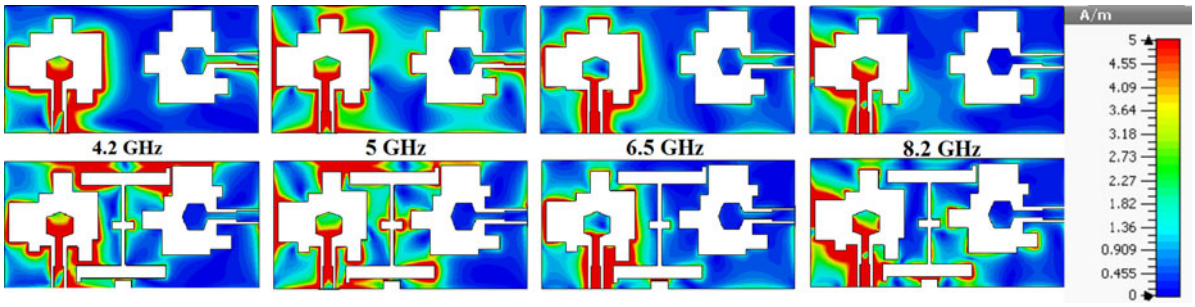

Fig. 4. Current distribution for port 1 of antenna 2 at 4.2, 5, 6.5, and 8.2 GHz.

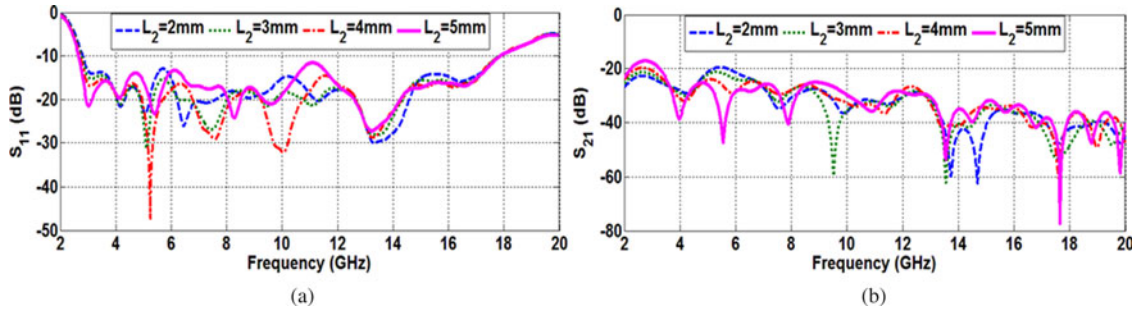

Fig. 5. Simulated results of (a) S_{11} and (b) S_{21} for different values of L_2.

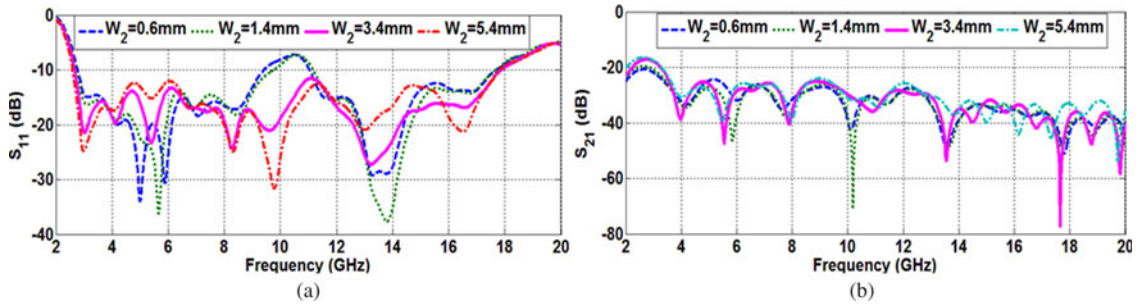

Fig. 6. Simulated results of (a) S_{11} and (b) S_{21} for different values of W_2.

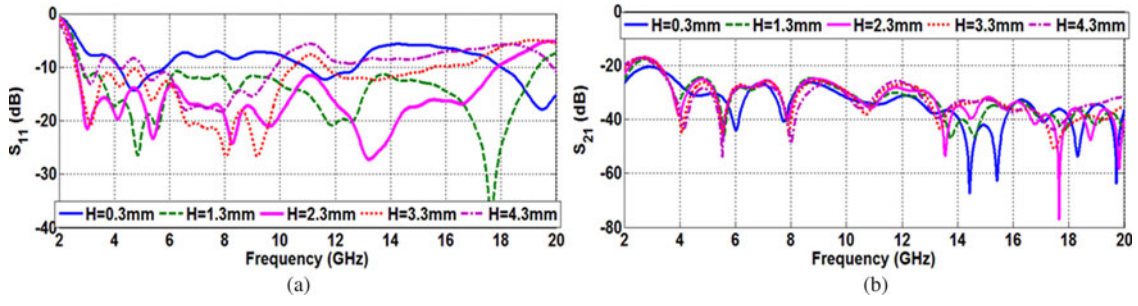

Fig. 7. Simulated results of (a) S_{11} and (b) S_{21} for different values of H.

return loss near 4.5 and 6.2 GHz. Width of the lower right stub is seen not to have much effect on the isolation (−ve of S_{21}) as seen from Fig. 7(b).

C) Height of the patch above the ground plane

The gap between the patch and the ground plane denoted by H is a very crucial parameter, hence its value is varied and return loss and isolation (−ve of S_{21}) are examined. This height controls the coupling between the radiating element of the antenna and the ground plane. For $H = 0.3$ mm, impedance matching deteriorates very badly as seen from Fig. 7(a). By gradually increasing the gap between the patch and the ground plane it is observed that, for $H = 1.3$ mm, the return loss slightly improves and by further increasing H to 2.3 mm, desired performance is achieved. But a still

https://doi.org/10.1017/S1759078715000975 Published online by Cambridge University Press

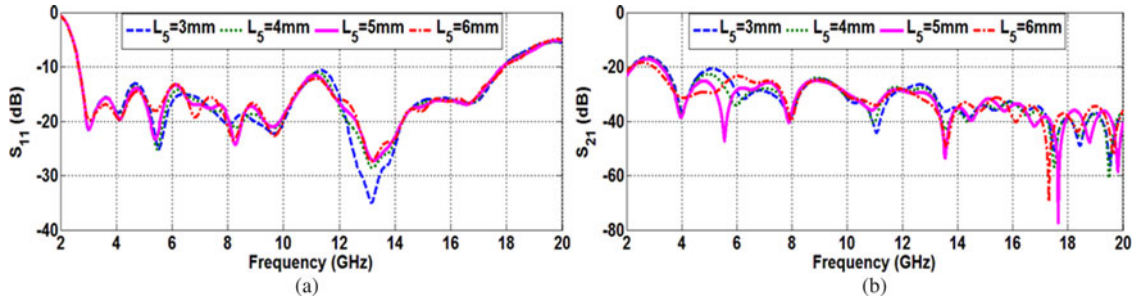

Fig. 8. Simulated results of (a) S_{11} and (b) S_{21} for different values of L_5.

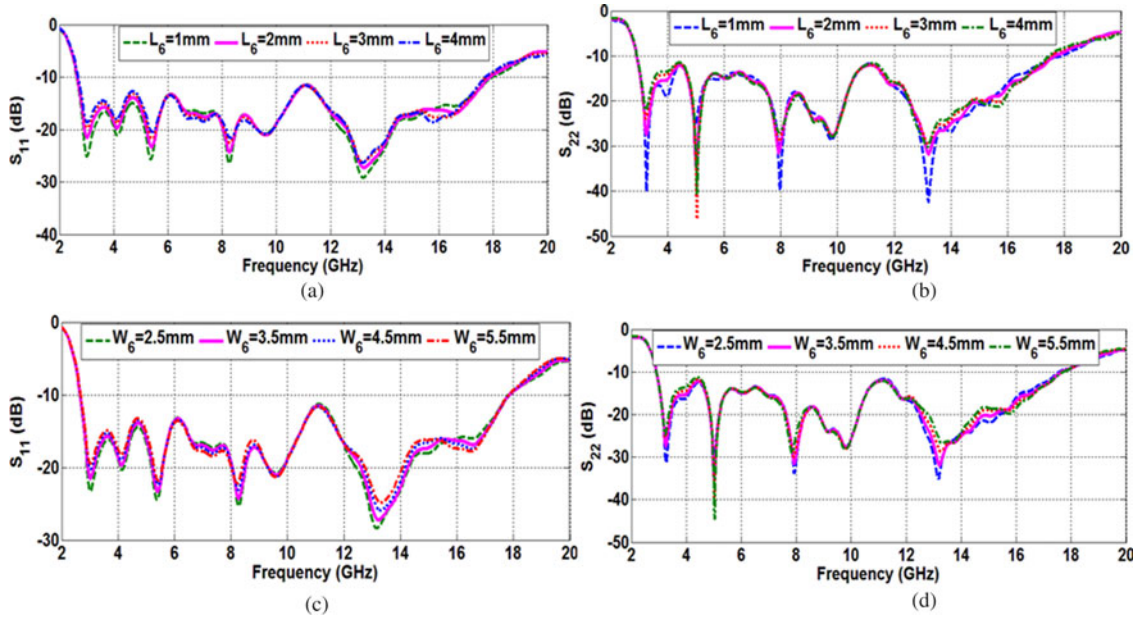

Fig. 9. Simulated results of (a), (c) S_{11} and (b), (d) S_{22} for different values of L_6 and W_6, respectively.

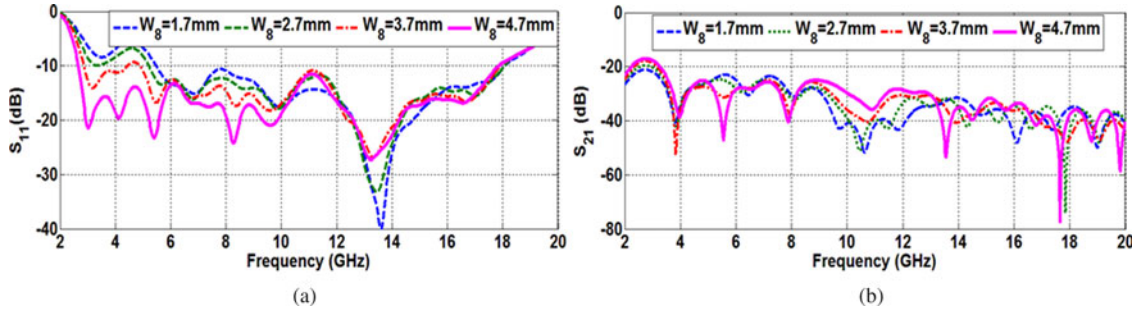

Fig. 10. Simulated results of (a) S_{11} and (b) S_{22} for different values of W_8.

further increase in H increases the return loss. The effect of the gap between the patch and the ground plane has not shown any adverse effect on isolation as seen from Fig. 7(b).

D) Height of top slot

The variations in return loss and isolation with length L_5 are shown in Fig. 8. As shown in Figs 8(a) and 8(b), L_5 does not have any much effect on the return loss or isolation. This is because of reduced current over this part of the antenna as seen from the current distribution plot (Fig. 4). At $L_5 =$ 3 mm, the return loss degraded at about 6.5 GHz. The isolation at $L_5 = 3$ mm is deteriorated at lower frequencies. Hence $L_5 = 5$ mm is taken as optimized value.

E) Height and width of upper left slot step

Figure 9 shows the effect of L_6 and W_6 on return loss and isolation. As shown in Figs 9(a) and 9(b), L_6 affects the return loss at lower frequencies and does not affect the isolation

https://doi.org/10.1017/S1759078715000975 Published online by Cambridge University Press

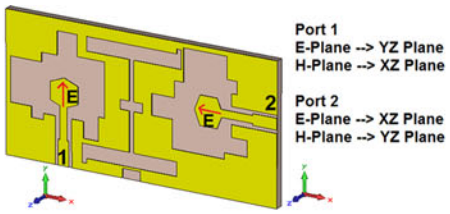

(a)

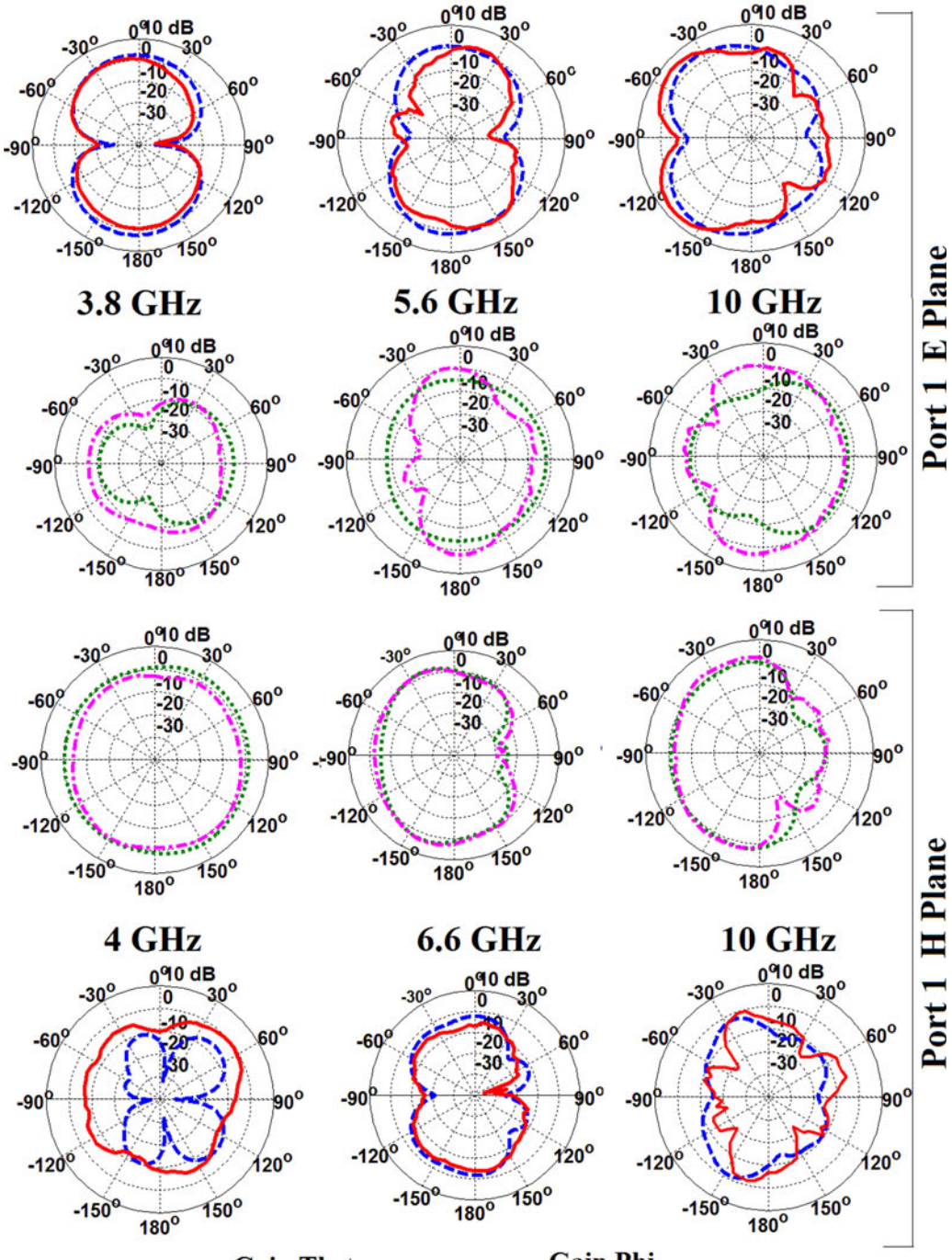

(b)

Fig. 11. (a) Placement of the two port antenna in the co-ordinate system and identification of the *E*- and *H*-planes for the two ports. (b) Measured and simulated radiation patterns of port 1. (c) Measured and simulated radiation patterns for port 2.

https://doi.org/10.1017/S1759078715000975 Published online by Cambridge University Press

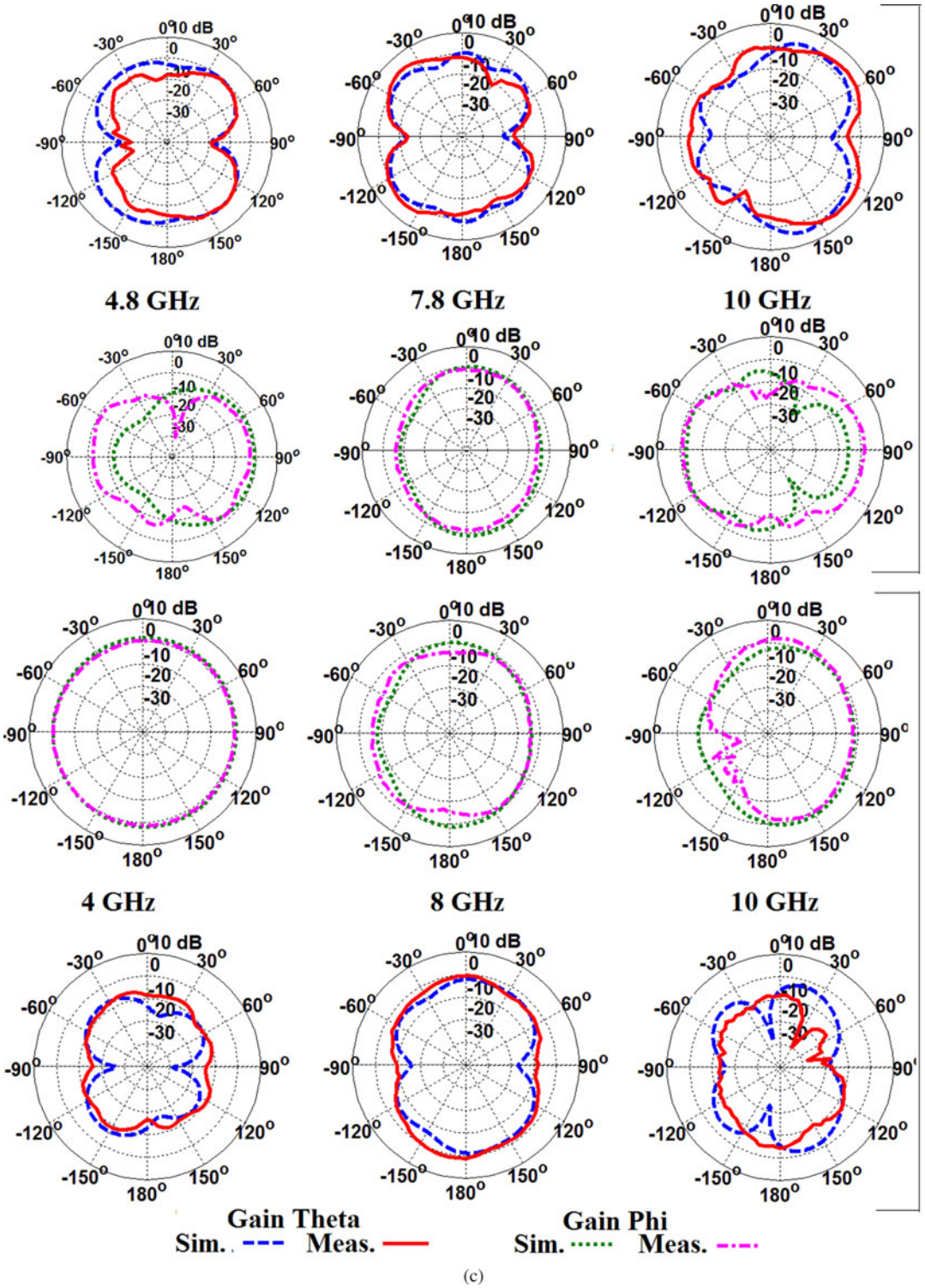

Fig. 11. (continued)

much. For a lower value of $L_6 = 1$ mm, the return loss for port 1 is slightly deteriorated. By increasing L_6, the return loss for port 1 is improved but for port 2 is deteriorated. Hence, an intermediate value of $L_6 = 2$ mm is fixed. The effect of various values of W_6 on the return loss and isolation is shown in Figs 9(c) and 9(d) and the effects are seen to be minimal. Again, the reduced effect of L_6 and W_6 on the return loss and isolation is due to the fact that little current is distributed around these parts.

F) Width of lower left ground stub

The parametric study of width W_8 is done and results are as shown in Fig. 10. The gap between the left side ground plane and the slot is examined. When $W_8 = 1.7$ mm, the impedance bandwidth is reduced, as W_8 is increased, the impedance bandwidth also increases simultaneously and for $W_8 = 4.7$ mm, the impedance bandwidth is found to be maximum along with good isolation.

https://doi.org/10.1017/S1759078715000975 Published online by Cambridge University Press

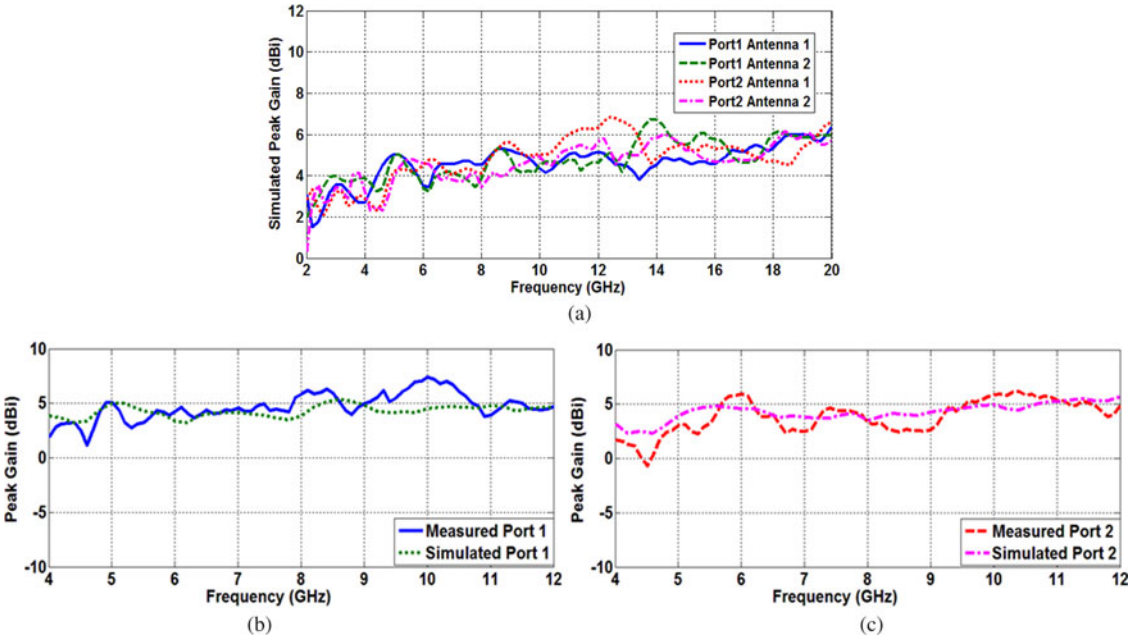

Fig. 12. Peak gains (a) simulated of both antennas, (b) measured and simulated of antenna 2, port 1, and (c) measured and simulated of antenna 2, port 1.

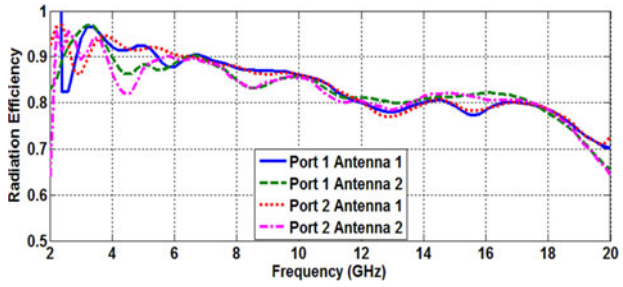

Fig. 13. Simulated radiation efficiency of antennas 1 and 2 for both the ports.

VII. RADIATION PATTERNS, PEAK GAIN, AND EFFICIENCY

The far-field performance of antenna 2 is studied and both the simulated and measured *E*- and *H*-plane radiation patterns for both the ports are shown in Fig. 11. The placement of the antenna in the co-ordiate system and the identification of the *E*-plane for the two ports is shown in Fig. 11(a). As shown in figure the *E*-plane for port 1 is the *YZ*-plane, whereas the *E*-plane for port 2 is the *XZ*-plane. The quadrature arrangement of the *E*-planes for the two ports indicates polarization diversity in the far-field patterns achieved with the proposed antenna.

Figure 11(b) shows the radiation pattern when port 1 was excited and port 2 was terminated by a 50 Ω line and Fig. 11(c) shows the radiation patterns when port 2 was excited. The radiation patterns at 4, 6, 8, 10, and 12 GHz were measured in the anechoic chamber. For *E*-plane of ports 1 and 2, the co- and cross-polarized components are the gain θ and gain ϕ components, while for the *H*-plane, the co- and cross-polarized components are the gain ϕ and gain θ components, respectively. The co-polarized gain in the *H*-plane has omni-directional pattern, while in the *E*-plane it shows dumb-bell-shaped nature.

The simulated peak gains of both the antennas and both the ports are compared in Fig. 12(a). The gains for both the ports for antennas 1 and 2 are between 3 and 6 dBi across the impedance bandwidth. For antenna 1, the peak gain for port 2 has gone up in the region of 10–14 GHz by approximately 2 dBi when compared with the peak gain at port 1. Similar increase is also noted for antenna 2.

The simulated and measured peak gains are compared and shown in Figs 12(b) and 12(c). The measured peak gain mostly shows good agreement with the simulated peak gain with a slight increase seen over the 9–11 GHz range. A few differences between the simulated and measured gains may be due to cable losses, SMA connector, and improper alignment of the antenna. The results are compared from 4 to 12 GHz because the horn antenna available for measurement of far-field radiation patterns works efficiently above 4 GHz.

VIII. RADIATION EFFICIENCY

The radiation efficiency is calculated by taking the ratio of the total power radiated from the antenna to the total input power. Hence, it gives the relation between the power delivered to the antenna and the power radiated by the antenna. The efficiency of an antenna must be as high as possible as it implies that most of the power present at the input of the antenna is radiated by it, whereas low efficiency implies that the power within the antenna is not radiated effectively due to impedance mismatch and losses. Figure 13 shows the radiation efficiency for antennas 1 and 2. It is above 85% at lower frequencies but it decreases to approximately 80% at higher frequencies due to increase in losses.

IX. DIVERSITY PARAMETERS

In a system-employing antenna diversity, the envelope correlation coefficient (ECC) is a very crucial parameter. In diversity

https://doi.org/10.1017/S1759078715000975 Published online by Cambridge University Press

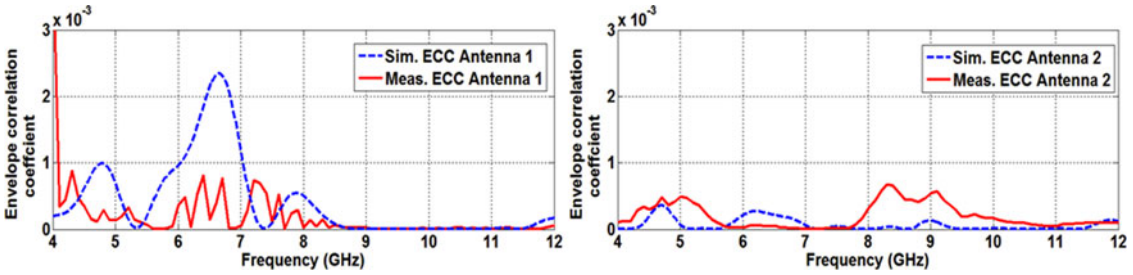

Fig. 14. Correlation coefficients (a) antenna 1 and (b) antenna 2.

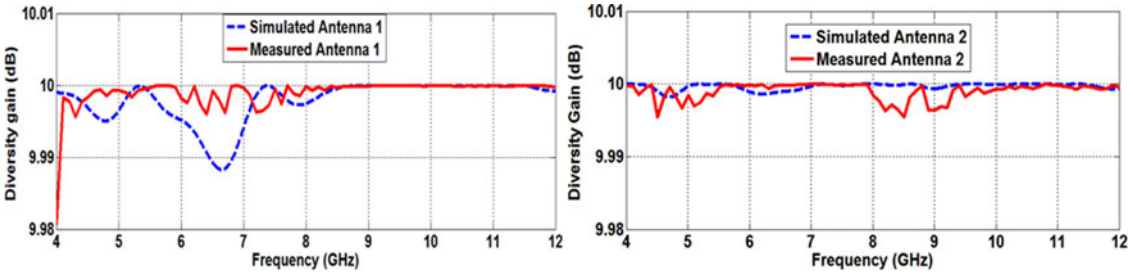

Fig. 15. Correlation coefficients (a) antenna 1 and (b) antenna 2.

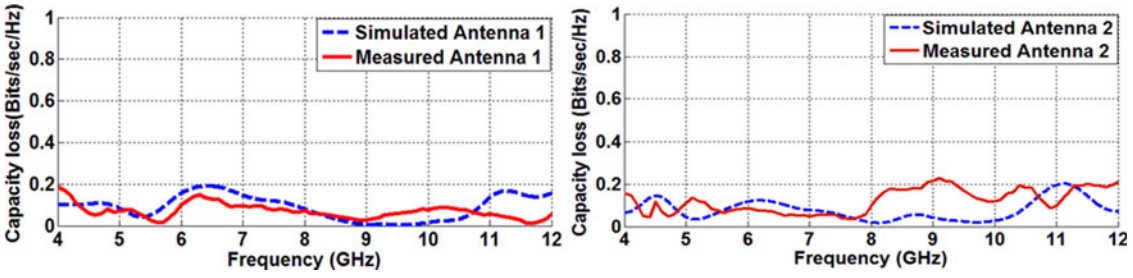

Fig. 16. Capacity loss (a) antenna 1 and (b) antenna 2.

antennas, signal from one port gets correlated to some extent with the signal at the other port; hence an evaluation of this degree of correlation becomes important. The ECC can be determined from equation (3) assuming the antenna array is placed in uniform scattering environment, antenna array is lossless structure and when one antenna is excited other is terminated by 50 Ω impedance [15]. For correlation between the signals to be less, the ECC value must be low. The ECC is calculated using scattering parameters as in equation (3). The *S*-parameters used in equation (3) are in linear values:

$$\rho = \frac{\left|S_{11}^{*}S_{21} + S_{12}^{*}S_{22}\right|^{2}}{\left|(1-|S_{11}|^{2}-|S_{21}|^{2})(1-|S_{22}|^{2}-|S_{12}|^{2})\right|}, \quad (3)$$

$$\rho = \frac{\left|S_{11}^{*} + S_{22}\right|^{2}}{\left|(|S_{11}|^{2})(|S_{22}|^{2})\right|}. \quad (4)$$

Under the conditions of no isolation ($S_{21} = 0$ dB), equation (3) reduces to equation (4). Further, if return losses at both the ports are equal, ρ will be a high value and will indicate high degree of mutual coupling between the two ports.

The simulated and measured ECCs are shown in Fig. 14. Both the simulated and the measured values are below 0.003 for antenna 1 and 0.0008 for antenna 2, this implies that very less correlation between signals in case of antenna 2 which provides better isolation also. The reference value for ECC is usually taken as 0.5 [9, 12].

Diversity gain is an another parameter for the diversity evaluation of the antenna. It is generally calculated using ECC (ρ_e) and is related as shown in equation (5). Diversity gain is obtained when value of ECC (ρ_e) is very low as possible. This implies that high isolation gives low ECC and good diversity gain. Figure 15 shows the diversity gain of both the antennas which are closer to 10:

$$G = 10\sqrt{1-|\rho_e|}. \quad (5)$$

Another useful parameter describing the performance of MIMO/diversity antenna is the capacity loss [14]. The capacity loss is calculated using equation (6):

$$C_{loss} = -\log_2 \det(A), \quad (6)$$

https://doi.org/10.1017/S1759078715000975 Published online by Cambridge University Press

where

$$A = \begin{bmatrix} \rho 11 & \rho 12 \\ \rho 21 & \rho 22 \end{bmatrix},$$

$$\rho_{ii} = 1 - \left(|S_{ii}|^2 + |S_{ij}|^2\right),$$

$$\rho_{ij} = -(S_{ii} \times S_{ij} + S_{ji} \times S_{ji}), \text{ for } i, j = 1 \text{ or } 2.$$

The value of capacity loss should be low. A low value indicates reliable transmission of data with little loss of information. In Fig. 16, the capacity loss for both the antennas is shown, it is found that the measured capacity loss is in agreement with the simulated capacity loss. The figure shows that the capacity loss for antennas 1 and 2 is below 0.2 bps/Hz.

X. CONCLUSIONS

This paper describes an UWB slot antenna for diversity applications. The overall antenna consists of two asymmetric rectangular slots orthogonally placed and excited by hexagonal patch. The isolation is improved by introduction of I-shaped slot stub between the two slot antennas. It is seen that whereas the isolation is better than 15 dB without the stub, it is brought above 25 dB over the entire band with the addition of the slot stub. The measured impedance bandwidth is from 3 to 12 GHz for both the designs. The radiation patterns, peak gain, and diversity parameters such as envelope correlation coeffcient and capacity loss are calculated and found to be within acceptable limits. Such type of antennas will be useful for WLAN, Wifi, and UWB portable devices requiring high speed and reliable data transfer.

ACKNOWLEDGEMENT

The second author acknowledges the financial support from DIAT (Deemed University), Pune, India.

REFERENCES

[1] Dagefu, F.T.; Oh, J.; Choi, J.; Sarabandi, K.: Measurements and physics-based analysis of co-located antenna pattern diversity system. IEEE Trans. Antennas Propag., **61** (11) (2013), 5724–5734.

[2] Kamarudin, M.R.; Nechayev, Y.I.; Hall, P.S.: Onbody diversity and angle-of-arrival measurement using a pattern switching antenna. IEEE Trans. Antennas Propag., **57** (4) (2009), 964–971.

[3] Zhao, H.; Zhang, F.; Zhang, X.; Wang, C.: A compact band-notched ultra-wideband spatial diversity antenna. Prog. Electromagn. Res. C, **51** (2014), 19–26.

[4] Azarmanesh, M.; Soltani, S.; Lotfi, P.: Design of an ultra-wideband monopole antenna with WiMAX, C and wireless local area network band notches. IET Microw. Antennas Propag., **5** (6) (2011), 728–733.

[5] Kharche, S.; Reddy, G.S.; Mukherjee, B.; Gupta, R.; Mukherjee, J.: MIMO antenna for bluetooth, wi-fi, wi-MAX and UWB applications. Prog. Electromagn. Res. C, **52** (2014), 53–62.

[6] Brown, T.W.C.; Saunders, S.R.; Evans, B.G.: Analysis of mobile terminal diversity antennas. IEE Proc. Microw. Antennas Propag., **152** (1) (2005), 1–6.

[7] Darvish, M.; Hassani, H.R.: Quad band CPW-fed monopole antenna for MIMO applications. EuCAP 2012, 1569522349, 1–4.

[8] Mohammad, S.; Nezhad, A.; Hassani, H.R.; Foudazi, A.: A dual band WLAN/UWB printed wide slot antenna for MIMO/diversity applications. Microw. Opt. Technol. Lett., **55** (3) (2013), 461–465.

[9] Nezhad, S.M.A.; Hassani, H.R.: A novel triband E-shaped printed monopole antenna for MIMO application. IEEE Antennas Wireless Propag. Lett., **9** (2010), 576–579.

[10] Najam, A.; Duroc, Y.; Tedjni, S.: UWB-MIMO antenna with novel stub structure. Prog. Electromagn. Res. C, **19** (2011), 245–257.

[11] Zhang, S.; Ying, Z.; Xiong, J.; He, S.: Ultrawideband MIMO/diversity antennas with a tree-like structure to enhance wideband isolation. IEEE Antennas Wireless Propag. Lett., **8** (2009), 1279–1282.

[12] Wong, K.; Su, S.; Kuo, Y.: A printed ultra-wideband diversity monopole antenna. Microw. Opt. Technol. Lett., **38** (4) (2003), 257–259.

[13] Hong, S.; Chung, K.; Lee, J.; Jung, S.; Lee, S.; Choi, J.: Design of a diversity antenna with stubs for UWB applications. Microw. Opt. Technol. Lett., **50** (5) (2008), 1352–1356.

[14] Votis, C.; Tatsis, G.; Kostarakis, P.: Envelope correlation parameter measurements in a MIMO antenna array configuration. Int. J. Commun. Netw. Syst. Sci., **3** (2010), 350–354.

[15] Singh, H.S.; Meruva, B.; Pandey, G.K.; Bharti, P.K.; Meshram, M.K.: Low mutual coupling between MIMO antennas by using two folded shorting strips. Prog. Electromagn. Res. B, **53** (2013), 205–221.

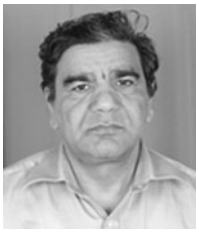

Raj Kumar was born on 14 May 1963 in Muzaffarnagar, UP, India. He completed his M.Sc. degree in Electronics in 1987 from the University of Meerut, Meerut, India. He was awarded the M.Tech. and Ph.D. degrees in Microwaves in 1992 and 1997, respectively, from the University of Delhi South Campus, New Delhi, India. He worked at CEERI, Pilani from 1993 to 1994 as a Research Associate. From May 1997 to June 1998, he worked as an Assistant Professor at Vellore College of Engineering (VIT), Vellore. He worked in DLRL (DRDO), Hyderabad as a Scientist from June 1998 to August 2002 and later on joined DIAT, Pune and worked in the Department of Electronics Engineering till September 2012. Since October 2012, he has been working in ARDE, Pune. His field of interest is microwave components, antennas, electromagnetic band-gap, frequency selective surface, filters, multiplexers, power dividers, couplers, numerical techniques, and ANN for microwave circuits and antennas.

Neha Pazare was born in Maharashtra, India, on 18 February 1990. She pursued Bachelor's degree in Electronics and Tele Communication from Rashtrasant Tukdoji Maharaj University, Nagpur, India in 2012. Currently, she is working toward M.Tech. degree from Defence Institute of Advanced Technology, Pune, India. Her research interests are in electromagnetics and microwave, ultra wideband antenna, multi-input multi-output antenna, and diversity antenna.

https://doi.org/10.1017/S1759078715000975 Published online by Cambridge University Press